Computing 72, 13–27 (2004)
Digital Object Identifier (DOI) 10.1007/s00607-003-0043-1

Computing
Printed in Austria

Planar Development of Free-Form Surfaces: Quality Evaluation and Visual Inspection

P. N. Azariadis and **N. S. Sapidis,** Ermoupolis

Received March 16, 2003; revised November 17, 2003
Published online: March 8, 2004

Abstract

Surface flattening is a crucial problem for many applications as indicated by the steady flow of new methods appearing in related publications. Quality control of these methods, by means of "accuracy criteria" independent of particular flattening methodologies, has not been addressed yet by researchers. This is exactly the subject of this paper: a detailed analysis of flattening is presented leading to geometric and physics-based criteria. These are implemented in intuitively-acceptable visualization techniques, which are applied to practical examples.

AMS Subject Classifications: 68U05, 68U07, 68U20, 65D17, 65D18.

Keywords: Planar developments, parameterizations, flattening accuracy, digital surfaces, isometry, isometric mapping, shape deformation, triangle-based surface representation, physics-based criteria, graphics-based methods.

1. Introduction

Construction of planar developments of free-form surfaces has attracted the interest of many researchers both in Manufacturing as well as in the Computer Graphics field. It is well known that it is possible to produce an isometric mapping of an arbitrary surface onto a plane only if this surface has everywhere zero Gaussian-curvature, i.e., it is *developable*. Recently, many methods for the approximate planar development of free-form surfaces have appeared focusing either on the fundamental flattening problem or on a specific application like *texture mapping*. In general, no unique solution to this problem exists. A common approach, followed by many researchers, uses a "custom" metric which is "optimally" preserved during surface flattening. Thus, the majority of the existing methods do not guarantee a generally-acceptable solution to the planar development problem.

As a result of all the above, the end-user has to select the "best solution" among a large number of flattening methods and eventually among many planar developments (resp. parameterizations) of a given surface. This selection must be based on a specific set of requirements imposed, for example, by product specifications. Published flattening methods and commercial software offer no adequate tools for

performing/supporting this task. These tools should be intuitively understood by the end-user and should provide local and/or global estimations of a development's quality. The introduction/derivation of such a set of tools and development of the related visualization techniques is the subject of this paper.

2. Current Methods for Approximate Flattening of Surfaces

The surfaces considered in this work are approximated with an adequate mesh $\mathbf{\Phi}$ of triangles. This mesh is allowed to have a variable density depending on the imposed accuracy criteria. Note that $\mathbf{\Phi}$ contains only "positive" non-degenerated triangles, i.e., their vertices have a counter-clockwise order so that the triangle area is always positive.

Ma and Lin [10] and later Maillot et al. [11] propose a flattening technique based on optimizing an objective function comparing the edge-length and triangle areas between corresponding triangles in $\mathbf{\Phi}$ and $\boldsymbol{\varphi}$. Azariadis and Aspragathos [2, 3] further improve the aforementioned method by modifying the area energy function and by giving a solution to the initial-guess problem. Employing the material properties of the initial surface, Shimada and Tada [17] proceed to developing a flattening method based on finite elements. Another method is proposed by Bennis et al. [4], where a relaxation procedure is used for the homogeneous distribution of deformation of the geodesic-curvature error in a planar development.

Yu et al. [20] present an algorithm using the in-plane strain related to the transformation of the curved surface to its planar development. Another approach [18] formulates the planar development problem using a spring-mass system and calculates the strain energy released during flattening. These authors also use a color graph to indicate areas where cutting lines should be introduced to release more strain energy but they use a very generic technique for measuring the flattening accuracy based on triangle edges and areas difference. The MIPS method [8] uses a more elaborated approach to measure the local isometry based on a non-linear energy which is invariant to orthogonal transformations and homogeneous scalings.

A method based on properties of the Gaussian curvature of a surface is proposed by Hinds et al. [7] aiming at planar developments for apparel design which are free of foldovers and are called "radial developments". McCartney et al. [12] offer another method, aiming again at the clothing industry, which handles insertion of darts and gussets by creating appropriate openings. Parida/Mudur [13] deal with the special case of composite materials and propose a robust flattening technique based on constraints. Azariadis/Aspragathos [1] extend this method to a general-purpose surface flattening technique divided into three-stages where the unfolding direction is taken into consideration by minimizing a local energy function.

Schwartz/Shaw/Wolfson [16] and Wolfson/Schwartz [19] use a special MDS (Multi-Dimensional Scaling) approach to flatten a curved surface utilizing geodesic distances. This method's computational complexity is very high, rendering it impractical. Zigelman et al. [21] improved this method by introducing a new

mapping technique that preserves both the local and the global structure of the planar development with minimal shearing effects. Sander/Snyder et al. [15] and Snyder/Gortler et al. [14] use a ''texture stretch'' metric based on singular values of the Jacobian of the affine mapping 2D-to-3D to compute a good parameterization. A drawback of this technique is that the boundary should be fixed and convex, imposing, thus, a large isometry error near boundary edges. Levy et al. [9] propose Least Squares Conformal Maps built on a criterion that minimizes angle deformations and non-uniform scalings. Desbrun et al. [5] developed a set of intrinsic parameterizations which preserve either angles (Discrete Conformal Mapping) or areas (Discrete Authalic Mapping) which are combined to form a general discrete parameterization method. They apply their theoretical results to parameterize 3D meshes with a fixed 2D boundary in the parametric space. They also show how to interactively optimize the boundary of the parameterization with respect to an appropriate energy. Conformal parameterizations have also been proposed by Eck et al. [6] who derived the linear condition for conformality using harmonic maps. Here again a fixed and convex boundary is required to produce conformal maps.

The above methods solve the surface development problem by using either ''custom'' energy models or geometrical properties of the surface. None of these methods estimates the quality of the planar development in relation to geometric or other criteria. They all rely on the assumption that, when the employed energy function is minimized, then an adequate planar development is derived. This is clearly not sufficient for the end-user who must perform a detailed quality-evaluation of the derived developments. To all our knowledge this is the first time that the notion of quality control of planar developments is proposed.

3. Geometric Quality Control of Planar Developments

3.1. Local Mappings between the Surface and its Planar Development

Let S be a surface given by the parametric equation $\mathbf{x} = \mathbf{x}(u, v)$ and the uv-plane P. Then, $\mathbf{x}^{-1}$ maps points of S onto the plane P. If $\mathbf{x}$ is an isometry then the surface S is developable. We focus on the opposite case where S is not developable, i.e., $\mathbf{x}$ is not an isometry. In this case, one of the methods of Section 2 is employed, which operates on a triangulation $\mathbf{\Phi}$ of S and produces a planar development on the plane P. The development is defined as a triangular mesh $\boldsymbol{\varphi}$ having equivalent topological characteristics with $\mathbf{\Phi}$. This section aims at producing methods and criteria to analyze $\boldsymbol{\varphi}$ as an approximation to an isometric development of $\mathbf{\Phi}$.

Let us consider an arbitrarily pair of corresponding triangles $\Delta(\mathbf{A}, \mathbf{B}, \mathbf{C})$ of $\mathbf{\Phi}$ and $\Delta(\mathbf{a}, \mathbf{b}, \mathbf{c})$ of $\boldsymbol{\varphi}$, where $\mathbf{A}, \mathbf{B}, \mathbf{C} \in \Re^3$ and $\mathbf{a}, \mathbf{b}, \mathbf{c} \in \Re^2$ are respectively the vertices of these triangles. We define their vertices through local orthonormal coordinate systems L and ℓ respectively as $\mathbf{A}^L = (0, 0)$, $\mathbf{B}^L = (B_x^L, 0)$, $\mathbf{C}^L = (C_x^L, C_y^L)$ and $\mathbf{a}^\ell = (0, 0)$, $\mathbf{b}^\ell = (b_x^\ell, 0)$, $\mathbf{c}^\ell = (c_x^\ell, c_y^\ell)$. The affine transformation from $\Delta(\mathbf{a}, \mathbf{b}, \mathbf{c})$ to $\Delta(\mathbf{A}, \mathbf{B}, \mathbf{C})$ is given by a local linear mapping $\mathbf{f}$ written in matrix form as

$$\begin{bmatrix} B_x^L & C_x^L \\ 0 & C_y^L \end{bmatrix} = \mathbf{f}\begin{bmatrix} b_x^\ell & c_x^\ell \\ 0 & c_y^\ell \end{bmatrix} \Rightarrow \mathbf{f} = \begin{bmatrix} \frac{B_x^L}{b_x^\ell} & \frac{b_x^\ell C_x^L - B_x^L c_x^\ell}{b_x^\ell c_y^\ell} \\ 0 & \frac{C_y^L}{c_y^\ell} \end{bmatrix} \tag{1}$$

Note that the matrix $\begin{bmatrix} b_x^\ell & c_x^\ell \\ 0 & c_y^\ell \end{bmatrix}$ always has an inverse since the determinant $D = b_x^\ell c_y^\ell$ is nonzero. The set of all local mappings **f** define the overall mapping of $\boldsymbol{\varphi}$ onto $\boldsymbol{\Phi}$. Thus, a detailed study of **f** is a prerequisite for the "isometry evaluation" of the development $\boldsymbol{\varphi}$.

3.2. Properties of Local Mappings

In this section we shall investigate both quantitative and qualitative characteristics of local mappings **f** in order to ascertain whether they define an isometry or not.

3.2.1. Local Isometry Examination

We can simplify the used notation taking into account that, since L and ℓ are orthonormal coordinate systems, we can express the coordinates of the vertices of $\Delta(\mathbf{A}, \mathbf{B}, \mathbf{C})$ and $\Delta(\mathbf{a}, \mathbf{b}, \mathbf{c})$ in a global coordinate system W as it is shown in Fig. 1:

$$\begin{aligned} \mathbf{A}^W &= (0,0), \quad \mathbf{B}^W = (B_x^L, 0), \quad \mathbf{C}^W = \left(C_x^L, C_y^L\right) \\ \mathbf{a}^W &= (0,0), \quad \mathbf{b}^W = (b_x^\ell, 0), \quad \mathbf{c}^W = \left(c_x^\ell, \quad c_y^\ell\right) \end{aligned} \tag{2}$$

Let $\mathbf{p}=$(x,y) be a point within $\Delta(\mathbf{a}^W, \mathbf{b}^W, \mathbf{c}^W)$. This point is mapped to a point $\mathbf{P}$ = (X,Y), within $\Delta(\mathbf{A}^W, \mathbf{B}^W, \mathbf{C}^W)$, according to $\mathbf{P} = \mathbf{fp}$. If **f** is an isometry then the squared Euclidean-distance between **p** and **P** should be zero, which is equivalent to having $f_{11} = 1$, $f_{22} = 1$ and $f_{12} = 0$. Thus, the only case where **f** causes no distortion is $\mathbf{f} = \mathbf{I_2}$.

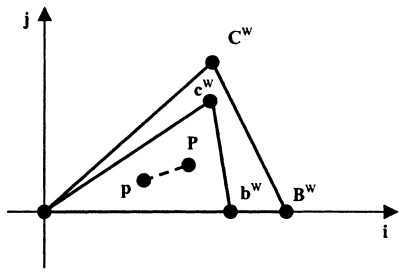

Fig. 1. The two corresponding triangles placed in the global coordinate system W with unit vectors $\mathbf{i}=(1,0)$ and $\mathbf{j}=(0,1)$

3.2.2. Deformation of a Unit Circle

A different configuration of the two triangles $\Delta(\mathbf{A},\mathbf{B},\mathbf{C})$ and $\Delta(\mathbf{a},\mathbf{b},\mathbf{c})$ is used with respect to a global orthonormal coordinate system W. The vertices of $\Delta(\mathbf{A},\mathbf{B},\mathbf{C})$ are defined according to Eq. (2) while the triangle $\Delta(\mathbf{a},\mathbf{b},\mathbf{c})$ is translated from its original location in $\boldsymbol{\varphi}$ by $-\mathbf{a}$:

$$\begin{aligned} \mathbf{A}^W &= (0,0), \quad \mathbf{B}^W = (B_x^W, 0), \quad \mathbf{C}^W = \left(C_x^W, C_y^W\right) \\ \mathbf{a}^W &= (0,0), \quad \mathbf{b}^W = (b_x^W, b_y^W), \quad \mathbf{c}^W = \left(c_x^W, c_y^W\right) \end{aligned} \tag{3}$$

This configuration is depicted in Fig. 2. In this case, the mapping $\mathbf{f}$ is given by

$$\mathbf{f} = \begin{bmatrix} \frac{B_x^W c_y^W - C_x^W b_y^W}{b_x^W c_y^W - b_y^W c_x^W} & \frac{b_x^W C_x^W - B_x^W c_x^W}{b_x^W c_y^W - b_y^W c_x^W} \\ -\frac{C_y^W b_y^W}{b_x^W c_y^W - b_y^W c_x^W} & \frac{C_y^W b_x^W}{b_x^W c_y^W - b_y^W c_x^W} \end{bmatrix} \tag{4}$$

Let us consider a circle $\mathbf{x_c}(\omega) = (x_c(\omega), y_c(\omega)) = (\cos\omega, \sin\omega)$ of unit radius with its center lying at the origin of the global system of reference. An arbitrarily circle point $\mathbf{x_c}(\omega) = (x_c(\omega), y_c(\omega))$ is mapped, through $\mathbf{f} = [f_{ij}]$, to a point $\mathbf{X}_c(\omega)$ according to

$$\begin{bmatrix} X_c(\omega) \\ Y_c(\omega) \end{bmatrix} = \begin{bmatrix} f_{11}\cos\omega + f_{12}\sin\omega \\ f_{21}\cos\omega + f_{22}\sin\omega \end{bmatrix} \tag{5}$$

Then, the squared distance between the new point $(X_c(\omega), Y_c(\omega))$ and the origin is

$$\begin{aligned} g(\omega) = X^2(\omega) + Y^2(\omega) &= (f_{11}^2 + f_{21}^2)\cos^2\omega \\ &+ (f_{12}^2 + f_{22}^2)\sin^2\omega + 2(f_{11}f_{12} + f_{21}f_{22})\cos\omega\sin\omega \end{aligned} \tag{6}$$

This distance should be equal to one for every $(X_c(\omega), Y_c(\omega))$ in order to avoid deformations. However, if $\mathbf{f}$ is not an isometry then deformations are unavoidable and the unit circle is deformed into an ellipse. The angle at which the unit circle undergoes the maximum or minimum deformation is computed at $g'(\omega) = 0$ as

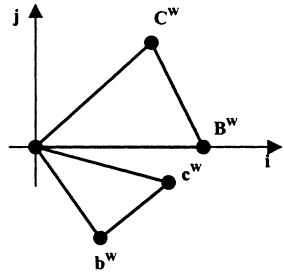

Fig. 2. The two corresponding triangles placed in the global coordinate system W with unit vectors $\mathbf{i}=(1,0)$ and $\mathbf{j}=(0,1)$

$$\omega_1 = \frac{1}{2}\tan^{-1}\frac{2(f_{11}f_{12} + f_{21}f_{22})}{f_{11}^2 + f_{21}^2 - f_{12}^2 - f_{22}^2} \tag{7}$$

Substituting Eq. (7) into Eq. (6), the principal direction of the ellipse relative to the x-axis of the frame W is given by

$$\beta = \tan^{-1}\frac{Y_c(\omega_1)}{X_c(\omega_1)} \tag{8}$$

The deformation of the unit circle along the first and second principal directions is

$$d_p = \sqrt{X_c^2(\omega_1) + Y_c^2(\omega_1)} \quad \text{and} \quad d_q = \sqrt{X_c^2(\omega_1 + \pi/2) + Y_c^2(\omega_1 + \pi/2)} \tag{9}$$

Remark 1. *The ellipse components (semiaxes) d_p and d_q are the square roots of the eigenvalues of the positive matrix* $\mathbf{ff^T}$.

Remark 2. *The mapping* $\mathbf{f}$ *is an isometry iff* $d_p = 1$ *and* $d_q = 1$.

3.3. Measuring the Accuracy of Planar Developments

The geometric accuracy of planar developments relates to measuring the metric distortion caused by the flattening process, which must be measured locally and globally. Trivial techniques for measuring accuracy, like triangle area, edge length and angles, provide only a quantitative evaluation of a development without being able to express qualitative properties like i.e. homogeneity or aspect ratio of the distortion. In addition, the measuring technique should be unaffected by translations, orthogonal transformations and by homogeneous scaling. The proposed indices take into account both quantitative and qualitative properties of planar developments.

3.3.1. Local Accuracy Measurement

Direct Triangle-Edge Difference: A straightforward measurement of the local accuracy is achieved by examining the difference in edge-lengths of corresponding triangles:

$$D(T) = \left|\frac{\|\mathbf{AB}\| - \|\mathbf{ab}\|}{\|\mathbf{AB}\|}\right| + \left|\frac{\|\mathbf{AC}\| - \|\mathbf{ac}\|}{\|\mathbf{AC}\|}\right| + \left|\frac{\|\mathbf{BC}\| - \|\mathbf{bc}\|}{\|\mathbf{BC}\|}\right|, \tag{10}$$

where $D(T) \in [0, +\infty)$ and $T = \Delta(\mathbf{A}, \mathbf{B}, \mathbf{C}) \in \mathbf{\Phi}$ with $\Delta(\mathbf{a}, \mathbf{b}, \mathbf{c})$ the corresponding triangle in $\boldsymbol{\varphi}$. The closer to zero $D(T)$ is, the lesser the local distortion in $\Delta(\mathbf{a}, \mathbf{b}, \mathbf{c})$.

Although $D(T)$ is not invariant to scaling, it can be used for a quick quantitative measurement of local isometry.

Homogeneity of Distortion: Since deformation is unavoidable in planar developments of free-form surfaces, it is important to examine whether this distortion is *homogeneously dispread* on the flattened surface, in order to avoid rapid changes in local accuracy and concentration of deformation in certain areas. This qualitative criterion can be defined as follows:

$$h(\mathbf{f}) = \left|d_p d_q - 1\right|, \quad h(\mathbf{f}) \in [0, +\infty) \tag{11}$$

Ideally, $h(\mathbf{f})$ should be equal to zero for an isometric mapping $\mathbf{f}$.

Aspect Ratio: Aspect ratio should be preserved to avoid non-uniform deformation of the planar development. This measurement is expressed as:

$$r(\mathbf{f}) = \left|\frac{d_p}{d_q} - 1\right|, \quad r(\mathbf{f}) \in [0, +\infty) \tag{12}$$

For an isometric mapping $\mathbf{f}$, $r(\mathbf{f})$ is equal to zero.

3.3.2. Global Accuracy Estimation

Global Triangle-Edge Difference: A global "isometry criterion" is directly derived by (10):

$$D = \sum_{T \in \mathbf{\Phi}} D(T), \quad D \in [0, +\infty) \tag{13}$$

Obviously, $D = 0$ is a necessary condition for $\boldsymbol{\varphi}$ to be an isometric mapping of $\mathbf{\Phi}$.

Global Homogeneity of Distortion: The ratio of $\min\{d_p d_q\}$ over $\max\{d_p d_q\}$, for all mappings, characterizes the global homogeneity of distortion in the planar development, i.e.,

$$h = \frac{\min\{d_p d_q\}}{\max\{d_p d_q\}}, \tag{14}$$

where $h \in (0, 1]$. Ideally, h should be equal to one.

Global Aspect Ratio: A global index characterizing the variation of aspect ratio on the entire planar surface is given by

$$r = \frac{\min\{d_q\}}{\max\{d_p\}}, \tag{15}$$

where $r \in (0, +\infty)$ and, ideally, r should be equal to one.

Table 1. Quality control results for the test cases.

Surface	Global homogeneity of distortion h	Global aspect ratio r	Min D(T)	Max D(T)	Min $h(\mathbf{f})$	Max $h(\mathbf{f})$	Min $r(\mathbf{f})$	Max $r(\mathbf{f})$
Torus (Fig. 3b)	5.98×10^{-1}	5.37×10^{-1}	6.35×10^{-3}	7.51×10^{-1}	4.70×10^{-5}	3.17×10^{-1}	3.11×10^{-3}	5.04×10^{-1}
Torus (Fig. 3c)	6.41×10^{-1}	6.87×10^{-1}	1.95×10^{-3}	4.65×10^{-1}	0	2.70×10^{-1}	1.46×10^{-3}	2.67×10^{-1}
Last	3.80×10^{-1}	6.90×10^{-1}	3.00×10^{-6}	5.89×10^{-1}	1.19×10^{-7}	1.20	6.55×10^{-7}	5.96×10^{-1}
Head	4.45×10^{-1}	2.74×10^{-1}	1.30	1.74	2.1625	6.10	1.22×10^{-3}	2.0981

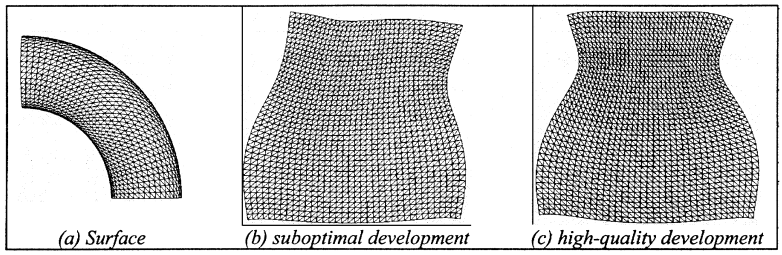

Fig. 3. Part of a torus surface with two corresponding planar developments

4. Physics-based Quality Control of Planar Developments

This section introduces an alternative methodology to evaluate developments as well as the related flattening-algorithms on the basis of the *forces* required to produce a planar development. This method is based on the error analysis of Section 3.2.2 and on the theory of Finite Elements Analysis (FEA). More specifically, in Section 3.2.2 we derived the deformation that each triangle in the flattened surface undergoes as a matrix product including two rotations and a deformation along principal directions. The first rotation is expressed through the angle β (Eq. (8)) and the components of the deformation by d_p and d_q (Eq. (9)). Using well-known results from FEA, we express this deformation in terms of nodal force-vectors (at the triangle vertices). In the plane stress problem, $\mathbf{B}$ is the strain matrix that contains the strain-nodal-displacement relationships, and $\mathbf{D}$ is the elasticity matrix representing stress-strain relationships for the surface's material. The nodal force-vector $\mathbf{g_f}$ implied by the deformation caused by $\mathbf{f}$ (Eq. (14)) is given by [17]

$$\mathbf{g_f} = \int_{\Delta} \mathbf{B}^{\mathrm{T}}\mathbf{D}\mathbf{T}\begin{pmatrix} d_p - 1 \\ d_q - 1 \\ 0 \end{pmatrix} dx\, dy = A\mathbf{B}^{\mathrm{T}}\mathbf{D}\mathbf{T}\begin{pmatrix} d_p - 1 \\ d_q - 1 \\ 0 \end{pmatrix}, \tag{16}$$

where A is the triangle's area and the orthogonal matrix $\mathbf{T}$ is given by

$$\mathbf{T} = \begin{bmatrix} \cos^2\beta & \sin^2\beta & -2\sin\beta\cos\beta \\ \sin^2\beta & \cos^2\beta & 2\sin\beta\cos\beta \\ \sin\beta\cos\beta & -\sin\beta\cos\beta & \cos^2\beta - \sin^2\beta \end{bmatrix} \tag{17}$$

Clearly, $\mathbf{g_f} = \mathbf{0}$ iff $\mathbf{f}$ is an isometry. It is proposed that nodal force-vectors are plotted on planar developments and are used as a secondary tool to locate excessive distortions; see examples in the next section.

5. Test cases[1]

5.1. Color Maps

All local, geometric accuracy-indices (Section 3.3.1) are presented to the user through appropriate color maps. More specifically, application of a particular quality criterion commences with calculation of the corresponding accuracy index at each vertex of a development through averaging of values produced by all triangles sharing this vertex. This value is then projected onto $[0, 1]$ interval and it is eventually associated to a color value expressed in grayscale. In all the examples presented in this section the darker the color, the higher the value of the associated index is.

5.2. Examples

The quality-control criteria and visualization methods, introduced in the previous sections of this paper, are applied to planar developments of varying quality to confirm/demonstrate their effectiveness in identifying inaccuracies. All numerical results related to the present examples are assembled in a single table (Table 1) to facilitate comparisons.

The first example is a torus part (Fig. 3). We perform quality control on two planar developments of this surface derived using the method [17]. In order to illustrate the effectiveness of the proposed tools in detecting accuracy problems, we produce (a) a suboptimal development by forcing the method to terminate prematurely, and (b) a high-quality development using the method appropriately. These are shown in Fig. 3.

For the suboptimal planar development (Fig. 3(b)): Since the local isometry index $D(T)$ takes values up to 0.75114, meaning that there exist triangles distorted up to 75%, it is evident that this planar development is not accurate. However, distortion is dispread within this planar development quite uniformly, except for the two dark areas in Fig. 4(a) where $h(\mathbf{f})$ reaches local maxima, i.e., there is a high concentration of deformation. Figure 4(b) depicts a color map of the local aspect ratio index $r(\mathbf{f})$ (Eq. (12)) together with the nodal forces (Section 4). It is obvious that significant distortion exists near the upper-right corner of the planar development, where also excessive stretching forces appear. In general, high $r(\mathbf{f})$ appears in areas where shear stress exists, as it is shown at the upper-right corner of Fig. 4b (right). *Conclusion: All criteria agree that the development in Fig. 3(b) is not accurate and thus inappropriate for applications*. To confirm this, we use this planar development to map a texture pattern onto the corresponding toroidal surface using the method [2]. The texture pattern is monochrome and consists of uniformly distributed black circular-disks. The texture mapped image (Fig. 4(c)) identifies vividly the parts of the surface corresponding to distorted areas of the planar development. Indeed, in the heavily distorted areas where $r(\mathbf{f})$ is high, the circles of the pattern are also

[1] Further material associated to the presented examples is available at http://www.syros.aegean.gr/users/azar/pub/pde.htm

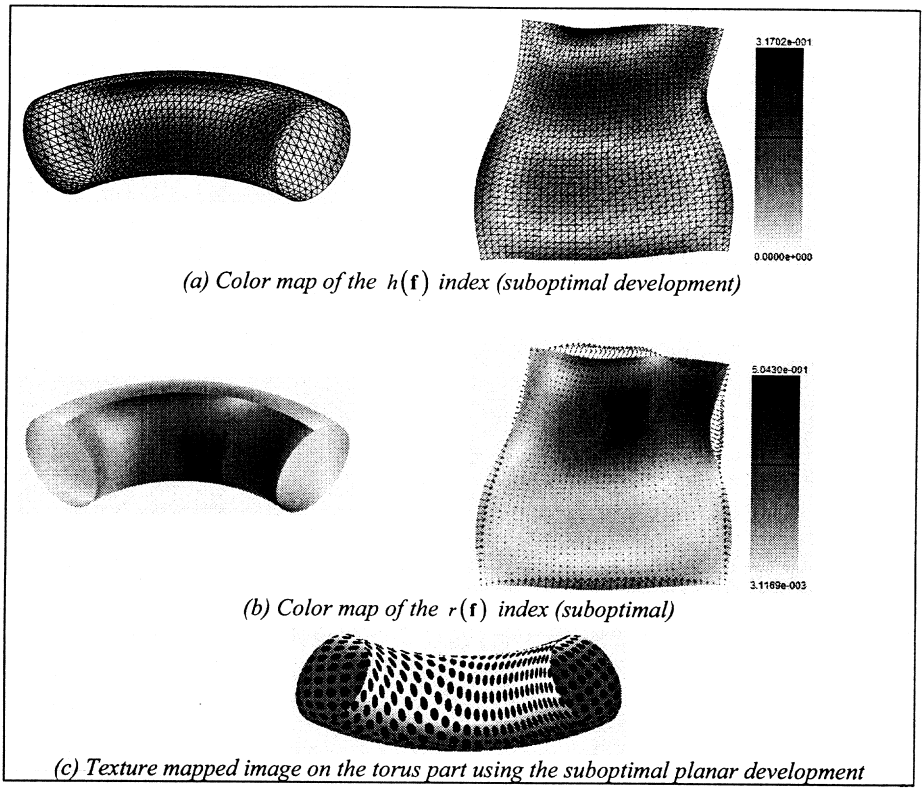

Fig. 4. The color maps corresponding to the suboptimal planar development of the torus (Fig. 3(b)). (a) Color map of the $h(\mathbf{f})$ index (suboptimal development). (b) Color map of the $r(\mathbf{f})$ index (suboptimal). (c) Texture mapped image on the torus part using the suboptimal planar development

distorted into elliptical shapes. It is interesting to note that the orientation of the "ellipses" agrees with that of the calculated nodal forces.

Applying the same quality-control methods on the second planar development (Fig. 3(c)) reveals its high quality/accuracy, indicated, e.g., by all indices in Table 1. Figure 5(a) (which is created using the same data range as the one used in Fig. 4(b)) agrees with this observation as the $r(\mathbf{f})$ value is significantly lower than that of Fig. 4(b). Furthermore, nodal forces along vertical boundaries appear almost symmetrical as one would expect based on the symmetry of the toroidal surface. However, there is an area near the middle of the horizontal boundaries where $r(\mathbf{f})$ is quite high, indicating a deformation of the aspect ratio. This deformation is confirmed by the texture mapped image (Fig. 5(b)), generated using this second development. Indeed, in Fig. 5(b) the result is quite satisfactory everywhere except for the indicated part corresponding to the area discussed above.

As a second test case we use an example from the footwear industry: flattening of the surface of a last (Fig. 6). We flatten the last using the global optimization method under constrains [3] making sure that the method terminates prematurely,

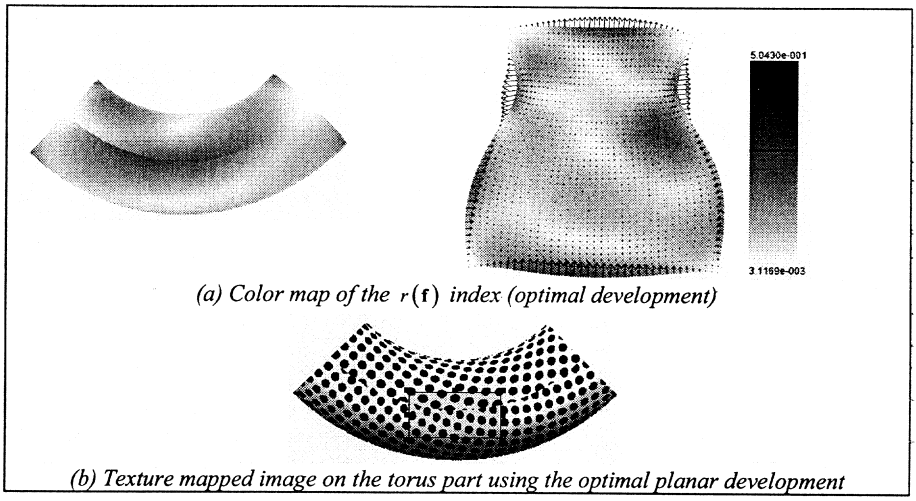

Fig. 5. Optimal planar development of the torus surface (Fig. 3c). (a) Color map of the $r(\mathbf{f})$ index (optimal development). (b) Texture mapped image on the torus part using the optimal planar development

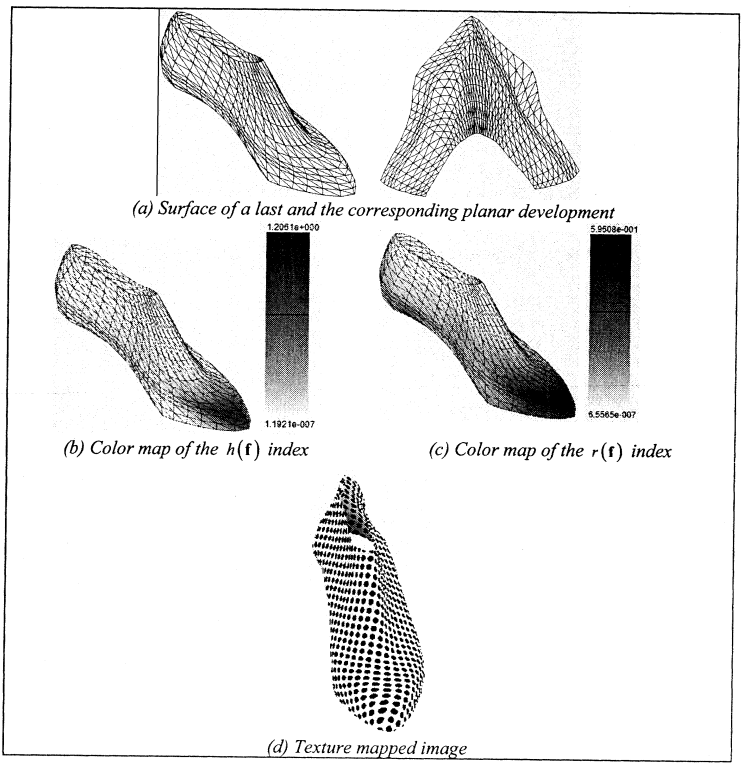

Fig. 6. The color maps of the last's surface. (a) Surface of a last and the corresponding planar development. (b) Color map of the $h(\mathbf{f})$ index. (c) Color map of the $r(\mathbf{f})$ index. (d) Texture mapped image

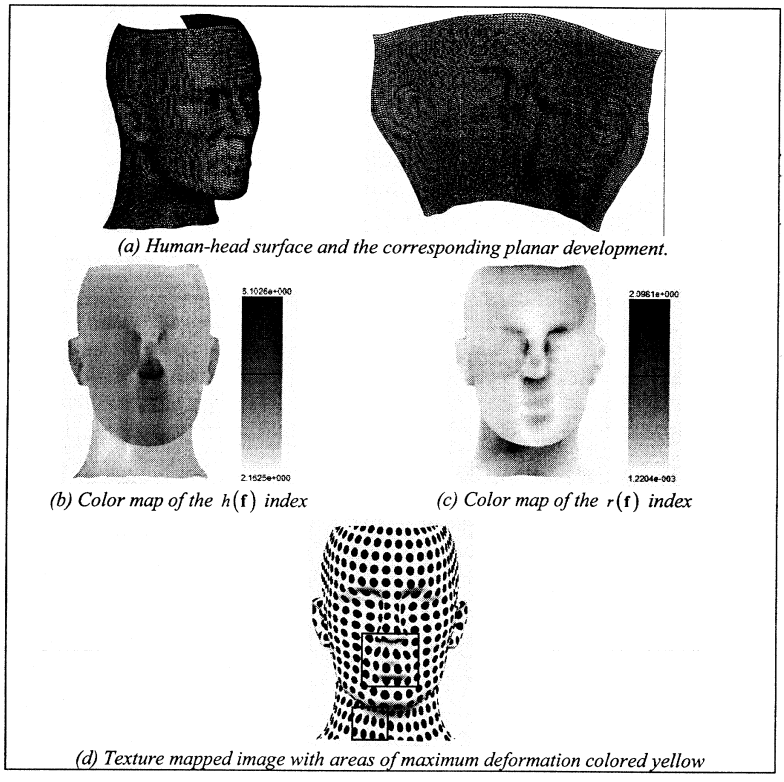

Fig. 7. Human-head surface and the corresponding planar development. (a) Human-head surface and the corresponding planar development. (b) Color map of the $h(\mathbf{f})$ index. (c) Color map of the $r(\mathbf{f})$ index. (d) Texture mapped image with areas of maximum deformation colored yellow

so that the result is not accurate; see Fig. 6(a). The numerical indicators in Table 1 agree with that; e.g., $D(T)$ indicates up to 58% distortion of triangle-edges. Furthermore, the color maps in Figs. 6(b) and 6(c) also identify inaccuracies at the forepart and at the perimeter of the surface, respectively. These results are empirically confirmed through the texture mapped image of the last illustrated in Fig. 6(d), where significant deformation of the pattern is shown at the forepart.

The third example tests our proposals on a highly complex surface, the human-head model in Fig. 7(a). The corresponding planar development is derived using the method [11]. All indices in Table 1 indicate significant inaccuracies in this development. The problematic areas are highlighted by the color maps of Figs. 7(b) and 7(c): The former points out inaccuracies at the area of the nose, while the latter indicates non-uniform deformations near the nose and in the neck area. These observations are empirically confirmed by texture mapping; see the two marked areas in Fig. 7(d).

6 Summary

Planar development of free-form surfaces is a classical problem in Computer-Aided Manufacturing with an increasing involvement in other fields like Computer Graphics. Currently, many solution-algorithms are available, forcing software-developers and end-users to seek criteria and methods to evaluate them. These "quality-control" criteria must focus on the fundamental features of planar development, being independent of the characteristics of any particular flattening method. This has been exactly the subject of the reported research that produced various geometric indices and one physics-based method to evaluate planar developments.

References

[1] Azariadis, P., Aspragathos, N.: Design of plane patterns of doubly curved surfaces. Computer-Aided Design *29*, 675–685 (1997).
[2] Azariadis, P., Aspragathos, N.: On using planar developments to perform texture mapping on arbitrarily curved surfaces. Computers & Graphics *24*, 539–554 (2000).
[3] Azariadis, P., Aspragathos, N.: Geodesic curvature preservation in surface flattening through constrained global optimization. Computer-Aided Design *33*, 581–591 (2001).
[4] Bennis, C., Vezien, J.-M., Iglesias, G.: Piecewise surface flattening for non-distorted texture mapping. Computer Graphics *25*, 237–246 (1991).
[5] Desbrun, M., Meyer, M., Alliez, P.: Intrinsic parameterizations of surface meshes. In: Drettakis, G., Seidel, H.-P. (eds.): Proceedings of Eurographics 2002, Computer Graphics forum, pp. 21, *3*, 210–218. Saarbrucken: Blackwell, 2002.
[6] Eck, M., DeRose, T., Duchamp, T., Hoppe, H., Lounsbery, M., Stuetzle, W.: Multiresolution analysis of arbitrary meshes. In: Proceedings of ACM SIGGRAPH 1995, Computer Graphics Proceedings, Annual Conference Proceedings, pp. 173–182, 1995.
[7] Hinds, B. K., McCartney, L., Woods, G.: Pattern development for 3D Surfaces. Computer-Aided Design *23*, 583–592 (1991).
[8] Hormann, K., Greiner, G.: MIPS – An efficient global parameterization method. In: Curve and Surface Design Conference Proceedings, pp. 153–162, 1999.
[9] Levy, B., Petitjean, S., Ray, N., Maillot, J.: Least squares conformal maps for automatic texture atlas generation. ACM Transactions on Graphics *21*, 362–371 (2002).
[10] Ma, S. D., Lin, H.: Optimal texture mapping. Proc. EUROGRAPHICS *88*, 421–428 (1988).
[11] Maillot, J., Yahia, H., Verroust, A.: Interactive texture mapping. Proc. SIGGRAPH 93, pp. 27–34. California: Anaheim 1993.
[12] McCartney, J., Hinds, B. K., Seow, B. L.: The flattening of triangulated surfaces incorporating darts and gussets. Computer-Aided Design *31*, 249–260 (1999).
[13] Parida, L., Mudur, S. P.: Constraint-satisfying planar development of complex surfaces. Computer-Aided Design *25*, 225–232 (1993).
[14] Sander, P., Gortler, S., Snyder, J., Hoppe, H.: Signal-specialized parameterization. In: Proceedings of Thirteen Eurographics Workshop on Rendering, pp. 87–98, 2002.
[15] Sander, P. V., Snyder, J., Gortler, S., Hoppe, H.: Texture mapping progressive meshes. In: Proceedings of ACM SIGGRAPH, Computer Graphics Proceedings, Annual Conference Proceedings, pp. 409–416, 2001.
[16] Schwartz, E. L., Shaw, A., Wolfson, E.: A numerical solution to the generalized mapmaker's problem: flattening nonconvex polyhedral surfaces. IEEE Trans. on Pattern Analysis and Machine Intelligence *11*, 1005–1008 (1989).
[17] Shimada, T., Tada, Y.: Approximate transformation of an arbitrary curved surface into a plane using dynamic programming. Computer-Aided Design *23*, 153–159 (1991).
[18] Wang, C., Chen, S.-F., Yuen, M.: Surface flattening for the fashion industry: a generic approach using Spring-Mass system. Computers in Industry 1548, 1–10 (2001).
[19] Wolfson, E., Schwartz, E. L.: Computing minimal distances on polyhedral surfaces. IEEE Trans. on Pattern Analysis and Machine Intelligence *11*, 1001–1005 (1989).
[20] Yu, G., Patrikalakis, N. M., Maekawa, T.: Optimal development of doubly curved surfaces. Computer Aided Geometric Design *17*, 545–577 (2000).

[21] Zigelman, G., Kimmel, R., Kiryati, N.: Texture mapping using surface flattening via multi-dimensional scaling. IEEE Trans. on Visualization and Computer Graphics *8*, 198–207 (2002).

Phillip N. Azariadis
Nickolas S. Sapidis
Department of Product &
Systems Design Engineering
University of the Aegean
Ermoupolis, Syros
84100 Greece
e-mails: azar@aegean.gr
sapidis@aegean.gr